Energy 239 (2022) 122255

Contents lists available at ScienceDirect

Energy

journal homepage: www.elsevier.com/locate/energy

High-temperature and radiation-resistant spinel-type ferrite coating for thermo-optical conversion in radioisotope thermophotovoltaic generators

Hongyu Wang [a], Zhiheng Xu [a, b], Zicheng Yuan [a], Kai Liu [a], Caifeng Meng [a], Xiaobin Tang [a, b, *]

[a] Department of Nuclear Science and Technology, Nanjing University of Aeronautics and Astronautics, Nanjing, 211106, China
[b] Key Laboratory of Nuclear Technology Application and Radiation Protection in Astronautics, Ministry of Industry and Information Technology, Nanjing, 211106, China

ARTICLE INFO

Article history:
Received 13 June 2021
Received in revised form
28 August 2021
Accepted 2 October 2021
Available online 7 October 2021

Keywords:
Radioisotope thermophotovoltaic
Gallium antimonide
Spinel-type ferrite coating
Radiation resistance
Thermo-optical conversion

ABSTRACT

High-temperature radioisotope heat source surface coated with excellent performance of thermo-optical conversion coating can greatly improve thermophotovoltaic energy utilization. However, long-term high-temperature and radiation resistance of the thermo-optical conversion pose a great challenge. In this work, spinel-type ferrite thermo-optical conversion coating was proposed to improve the heat and irradiation stability and output power of a radioisotope thermophotovoltaic (RTPV) prototype. Under the continuous irradiation of 32.64 kGy for 24 h at 1400 K, the emissivity of the spinel-type ferrite thermo-optical conversion coating could maintain more than 90%. In addition, the surface morphology of the coating was changed under high temperature, which enhanced its surface emissivity. Spinel-type ferrite thermo-optical conversion coating was applied to the RTPV prototype, which achieved a maximum output power of 144.23 mW. Compared with the RTPV prototype without coating, the overall output increased to 181.51%. Spinel-type ferrite thermo-optical conversion coating showed great application potential in the fields of thermo-optical conversion and high-efficiency utilization of thermal energy.

1. Introduction

In the recent decade, the rapid development of deep-space exploration has aroused an urgent need for high-reliability power system [1,2]. For space power systems, energy conversion systems operating in solid state are relatively more stable and reliable [3–5]. Thermophotovoltaic (TPV) is a stable solid-state, energy conversion, and thermal-to-electricity technology. Its main components and working principle indicate that the thermal at the hot side of the system is transferred through infrared radiation, and then the TPV cell at the receiving end converts infrared-light energy into electric energy through the photovoltaic effect [6–10]. Converting heat energy of the radioisotope heat source into electric energy by TPV technology leads to high specific power, stability, and long life. At present, compared with the application of relatively mature thermoelectric (TE), the TPV experimental efficiency of TE photovoltaic is generally above 10%, which can even reach 24.1% [11], and the power density can reach 3–4 times that of TE. Therefore, TPV has great application potential in long-term deep-space exploration [12–14].

At present, the mature application of radioisotope heat sources is the general-purpose heat source (GPHS) proposed by the National Aeronautics and Space Administration. Given the extensive and successful application of GPHS in recent space missions, it can be used as a reference for the specific parameters of RTPV heat source. The surface of the current radioisotopic heat pellets is usually covered by low-emissivity metal or ceramic body oxides [15]. If thermal energy is converted into light directly through the low-emissivity surface of the heat source, then achieving high-efficiency advantages of TPV technology becomes difficult. Therefore, the surface of the radioisotope heat source must add an efficient thermo-optical conversion coating as emitters to improve the infrared-light emission efficiency of the surface of the radioisotope heat source [16,17]. The GPHS operating temperature range of the

* Corresponding author. Department of Nuclear Science and Technology, Nanjing University of Aeronautics and Astronautics, Nanjing, 211106, China.
E-mail address: tangxiaobin@nuaa.edu.cn (X. Tang).

https://doi.org/10.1016/j.energy.2021.122255
0360-5442/

Nomenclature

b	Wien's displacement constant, nm K^{-1}
c	Speed of light, m s^{-1}
h	Planck's constant
I	Output current of the radioisotope thermophotovoltaic (RTPV), mA
I_{sc}	Short-circuit current of the RTPV, mA
P	Power of the RTPV, mW
k	Boltzmann constant
$M(\lambda)$	Power density of blackbody radiation, mW cm^{-1}
P_{out}	Output power of the RTPV, mW
P_{max}	Maximum output power of the RTPV, mW
T	Surface temperature of heat source, K
V	Output voltage of the RTPV, V
V_{oc}	Open-circuit voltage of the RTPV, V
ε_c	Surface emissivity

surface is usually 1273 K−1343 K [18,19], and the irradiation effect of high-energy rays also exists. The initial deposition dose on the surface of a 500 W GPHS heat source is approximately 0.135 Gy/h [20,21]. Therefore, in actual work, the thermo-optical conversion coating of the radioisotope thermo-photoelectric generator is continuously affected by high-temperature and radiation factors, and the emissivity of most metal functional materials will decrease or even fail [7]. Therefore, analyzing the thermo-optical conversion performance and long-term functionality of the material in the environment is necessary.

Currently, rare-earth materials are typical thermal radiation materials for thermal photovoltaic systems because of their excellent chemical and thermal stability [22]. However, they have a narrow emission peak and low overall spectral power, which lead to the poor overall performance of TPV. In addition, using photonic crystals and metamaterials as emitters on the surface of TPV heat sources is a novel research idea [23–26]. Given the good spectral selective emission capability and high theoretical energy conversion efficiency, these materials have excellent application prospects in TPV systems. However, the effects of the above-mentioned materials on the irradiation from the heat source have not been deeply considered and studied. Previous studies have explored the strong infrared emission performance and application of organosilicon coatings, but seldom involved its high temperature and radiation resistance [17]. Therefore, developing highly stable materials with high temperature and radiation based on a radioisotope heat source is necessary, which can be used as thermo-optical conversion coating for RTPV. The spinel-type ferrite is a metal oxide material with high melting point, high structure, and stable chemical properties. Given its high-temperature resistance and high emissivity, the spinel-type ferrite is suitable for thermal photovoltaic systems. Meanwhile, the spinel-type ferrite is widely used in aerospace, metallurgy, and other high-temperature insulation fields [27,28].

In this work, the Cu-spinel-type ferrite coating was used as the thermo-optical conversion layer for isotope heat source. In addition, it was applied to RTPV to achieve stable and efficient infrared emission and improve the power output. Long-term high temperature heating and ray irradiation experiments on spinel-type ferrite thermo-optical conversion (SFTOC) coating were further carried out, and compared and analyzed the changes in the emissivity and microstructure of SFTOC. Moreover, the prepared SFTOC was coated on the equivalent heat source of electric heating and assembled into an RTPV prototype. The performance of the integrated RTPV prototype under different heat source temperatures was tested experimentally. High-temperature cycling experiment was designed to prove its stability. The obtained results show that the prepared SFTOC has excellent thermo-optical conversion characteristics, and can has potential application prospects in the long-life space nuclear power supplies with long-term high temperature and radiation.

2. Materials and methods

2.1. Synthesis and preparation of SFTOC coating

The preparation of SFTOC powders: NiO (1 mol), Fe_2O_3 (1 mol), and anhydrous ethanol (20 ml) were added to the planetary ball mill and then ground at 200 r/min for 8 h. The ball-milled slurry was dried to obtain uniform powders in an air drying oven at 80 °C. The dried powder mixture was calcined in a tubular furnace (OTF-1200X) at 1100 °C for 3 h. High temperature solid phase synthesis reaction takes place at high temperature to form spinel structure. After falling to room temperature, the calcined powder sample was ground and then passed through a 500-mesh stainless steel screen to obtain the required $NiFe_2O_4$ powders. The $CoFe_2O_4$ and $CuFe_2O_4$ powders can be obtained by substituting CoO and CuO for NiO, respectively. The other preparation processes were the same as previously described.

The preparation of slurry: Ethyl cellulose (3 wt% SFTOC powders) was used as additives to increase the viscosity of the coating. Terpineol (52 wt% SFTOC powders) was used as a solvent. BYK-110 (2 wt% SFTOC powders) was used as a dispersant to obtain a suspension of ceramic particles in the paste. SiO_2–ZnO–B_2O_3 (3 wt% SFTOC powders) was used as an inorganic silicate binder to mark the filler bond to each other and to the matrix material after high-temperature annealing.

The above-mentioned raw materials were mixed to prepare the paste, and an appropriate amount of anhydrous ethanol was added to the paste, which was stirred in a planetary mixer at 80 °C for 20 min and then stirred at room temperature for 2 h to obtain the SFTOC paste.

Al_2O_3 has an excellent heat resistance, and it is often used as a protective layer on the surface of heat emitters. Thus, we used Al_2O_3 as substrate and primary comparison sample. Firstly, the Al_2O_3 substrate (Round, diameter 8 mm, thickness 1 mm) is placed into anhydrous ethanol, and ultrasonic cleaning is performed for 30 min. After cleaning, the substrate was dried in an oven at 80 °C for 30 min. The prepared SFTOC paste was applied to the Al_2O_3 substrate for 30 s at a speed of 3000 r/min on the spinning coater, and then the coating was removed and left standing for 5 h to dry evenly (Fig. 1). Afterward, the SFTOC coating was dried in an oven at 80 °C for 1 h, annealed in a tubular furnace at 1100 °C for 2 h, and then slowly lowered to room temperature in the furnace body to obtain the required SFTOC layer. The average measured thickness of

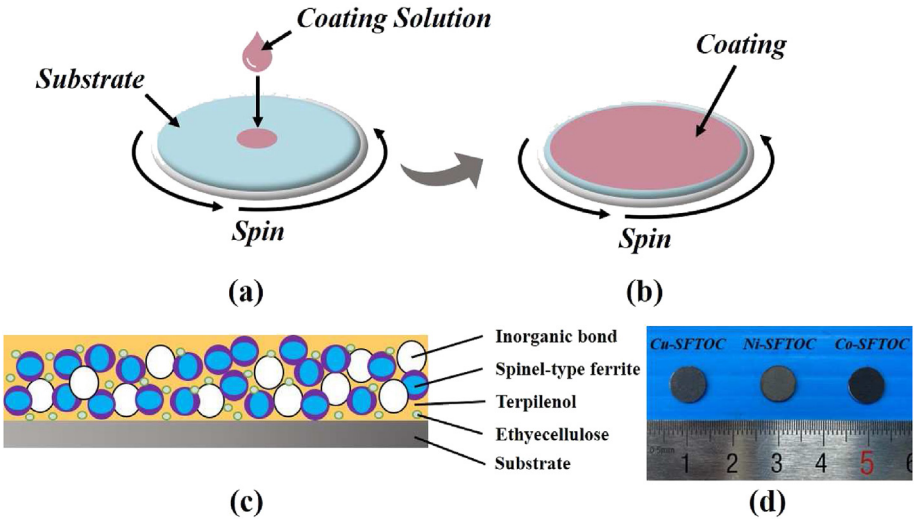

Fig. 1. (a–b) Method of spin coating to SFTOC coating, (c) sintering before the coating structure diagram, and (d) sintering after the actual drawing.

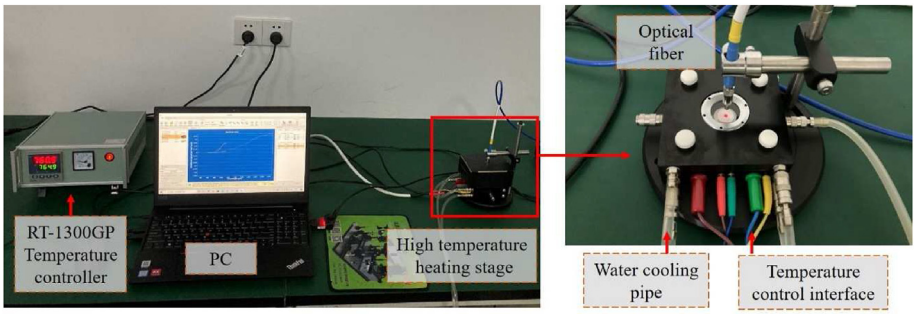

Fig. 2. Emission spectral test platform for SFTOC coating.

SFTOC was 62 μm (Fig. 1[d]). In addition, the SFTOC coating was fabricated on a cylindrical heat source with curved surface for experimental testing on an RTPV prototype. First, the initial cylindrical heat source rod was ultrasonic cleaned in anhydrous ethanol for 30min, and then dried in the air-blast drying oven. The treated cylindrical heat source rod was soaked into the prepared SFTOC slurry. After standing for 5 min, the SFTOCC coating machine was slowly pulled at the speed of 1 cm/min, and the uniform SFTOCC coating was coated on the heat source rod. The obtained cylindrical heat source coating was left standing for 5 h at room temperature, and then dried for 1 h in a drying oven with air blast at 80 °C. The coating needs to be annealed in a tubular furnace at 1100 °C for 2 h too. The final SFTOC coating heat source rod was obtained after the sample was taken out slowly at room temperature in the furnace body.

2.2. Characterization of SFTOC powder and coating emissivity

X-ray diffraction (XRD) patterns were obtained by using Cu Kα X-ray source at 40 kV and 40 mA. The morphologies of the materials were imaged using Quanta 650 FEG scanning electron microscope (SEM, Thermo Fisher Scientific) operating at 15 kV. The reflectivity of the coated SFTOC was obtained at room temperature was tested by the UV–Vis–NIR spectrophotometer (Cary 5000), and the emissivity of the samples was calculated according to Kirchhoff's law [29]. At thermal equilibrium, body's emissivity $\varepsilon_C(\lambda)$ at each wavelength was equal to its absorptivity $\alpha(\lambda)$. According to Equation (1), emissivity can be obtained indirectly by calculating the reflectivity $R(\lambda)$ and transmittance $T(\lambda)$ of the object. In SFTOC coating with considerable thickness, $T(\lambda)$ was equal to 0,

$$\varepsilon_C(\lambda) = \alpha(\lambda) = 1 - R(\lambda) - T(\lambda) \quad (1)$$

2.3. Experimental methods for tolerance testing of SFTOC coating

In reaching the temperature of the actual GPHS heat source, the prepared SFTOC coating was placed in a high-temperature muffle furnace, maintained at 1400 K for 24 h, and collected after cooling. In obtaining the external radiation characteristics of the GPHS heat source, the radiation tolerance experiment of the SFTOC coating was conducted at the ^{60}Co Radiation Center of Nanjing University of Aeronautics and Astronautics. Under the γ radiation field with

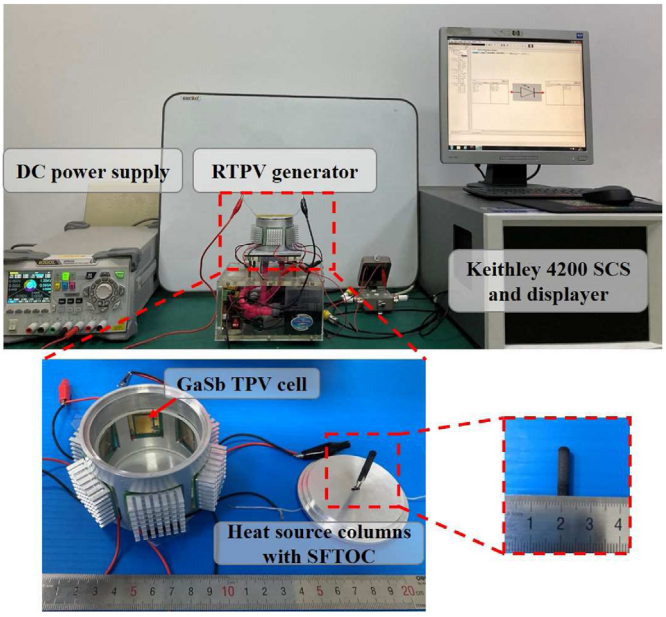

Fig. 3. RTPV prototype and experiment.

photon energy of 1.17 and 1.33 MeV, the dose rate sites of 0.68 kGy/h were selected. In the experiment, based on the dose rate of the heat source surface (0.135 Gy/h), SFTOC coating was irradiated for 48 h, attributing to 27.6 yr of working time.

2.4. Test methods for the thermo-optical conversion of SFTOC coating

The thermo-optical conversion properties can be intuitively evaluated by the spectral emission curve of materials at high temperature. SFTOC coating was heated to 1300 K by high-temperature hot bench (RT1300-GP), and the heating rate was 40 K/min. In addition, the heated SFTOC coating was evaluated by a near-infrared spectrometer (NIR2500, Shanghai Fuxiang Optical Co., Ltd.; Fig. 2). The GaSb ($E_g = 0.72$ eV) TPV cell with an effective area of 11.05 × 16.51 mm^2 was used as the follow-up photoelectric test and was directly fabricated on the printed circuit board substrate.

The infrared radiation spectrum of SFTOC at high temperature was related to its surface emissivity $\varepsilon_c(\lambda)$ and surface temperature, as shown in Planck's law [30] (Equation (2)) [10], where h is the Planck's constant; k is the Boltzmann constant; c is the speed of light; T is the surface temperature of the heat source; λ is the infrared spectrum wavelength.

$$M(\lambda) = \varepsilon_c(\lambda) \frac{2\pi hc^2}{\lambda^5 \left(e^{\left(\frac{hc}{\lambda kT}\right)} - 1 \right)} \tag{2}$$

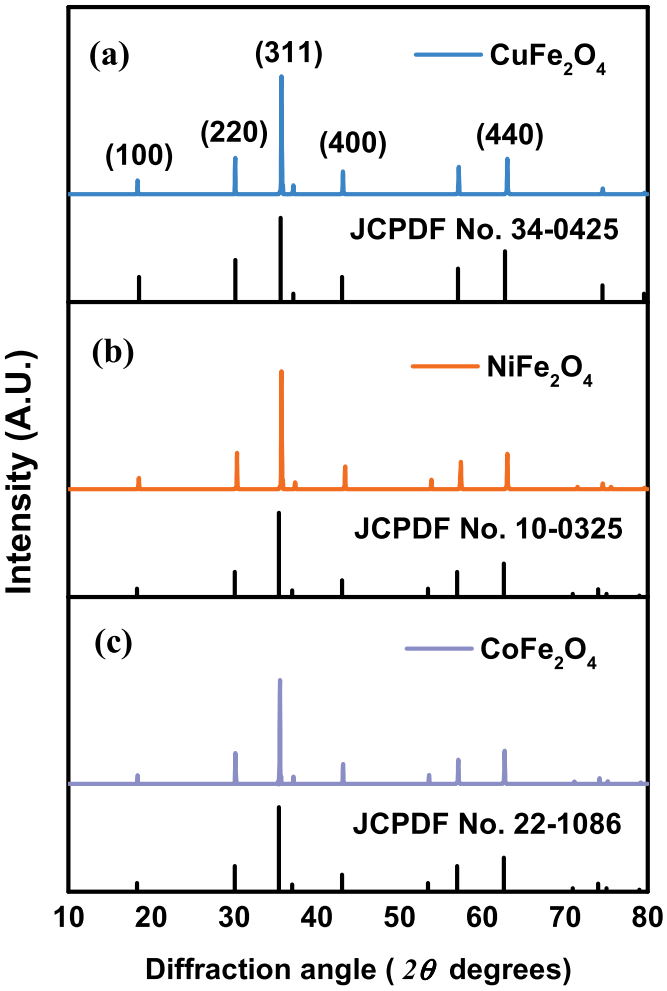

Fig. 4. XRD spectra of (a) $CuFe_2O_4$, (b) $NiFe_2O_4$, and (c) $CoFe_2O_4$ SFTOC powders.

2.5. Structural and test method for RTPV prototype with SFTOC

Fig. 3 shows the RTPV model for online testing via the parameter analyzer, and a resistive Joule thermal surrogate was used in the RTPV to simulate a radioactive fuel pellet for experimental research. The SFTOC paste was coated on the equivalent fuel pellet surface in RTPV and conducted high-temperature adhesion treatment. The power for the heat source rods was provided by a programmable linear DC power supply (DP832A, RIGOL Technologies Inc.). The temperature range of 700 K–1000 K represents the heat source columns. The temperature of the heat source was obtained using a temperature-measuring instrument (Agilent 34970A Data Acquisition with 34901A 20 Channel Multiplexer). Six pieces of GaSb TPV cells were connected in series inside the RTPV shell, which were 3.5 cm away from the heat source, and the fins on the back of the TPV cells were used to heat the TPV cell. The electrical performances of the RTPV were tested by a parameter analyzer (Keithley 4200 SCS) in a dark environment with a normal temperature of

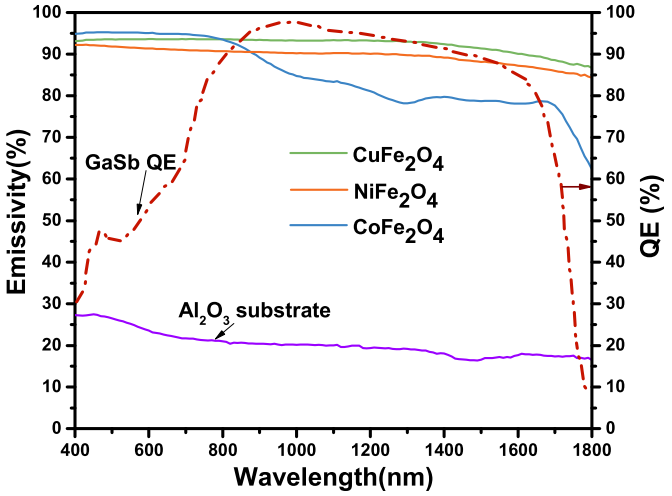

Fig. 5. Emissivity of three types of SFTOC coating and GaSb quantum efficiency curve.

293.15 K and a standard atmospheric pressure of 1 atm.

3. Result and discussion

3.1. Material property analysis of SFTOC coating

Fig. 4(a–c) show the XRD spectra of $CuFe_2O_4$, $NiFe_2O_4$, and $CoFe_2O_4$ SFTOC powder samples. The XRD peaks of the SFTOC powders can be indexed to the corresponding JCPDF crystal samples (JCPDF Nos. 34–0425, 10–0325, and 22–1086). The element types and content are consistent with raw material powder. This result also proves that the required SFTOC material can be prepared by the high-temperature solid-phase method.

Fig. 5 shows the three kinds of SFTOC coating emissivity curves. In the wavelength range of 400–1800 nm, the emissivity of Cu-SFTOC and Ni-SFTOC coating was maintained at approximately 80%–90%. Compared with Al_2O_3 substrate, the emissivity is greatly improved. SFTOC had a high emissivity in the response band (400–1800 nm) of the GaSb TPV cell, which can provide higher photocurrent density and electrical output power to RTPV. Compared with Ni-SFTOC coating, the emissivity of Cu-SFTOC coating was approximately 5% higher in the wavelength range of 600–1800 nm. The emissivity of Co-SFTOC was up to 95% in the visible and near-infrared band (in the wavelength range of 400–800 nm), but it began to decline in the wavelength range of 900–1800 nm. However, the emissivity of Co-SFTOC attenuation was located in the high photoelectric response range of the GaSb TPV cell. Thus, the application of Co-SFTOC in RTPV was slightly inferior to Cu-SFTOC and Ni-SFTOC coating.

3.2. Electrical properties of SFTOC coatings used in the RTPV

The reflectivity of SCTOC coating was tested at room temperature and the emissivity of SCTOC coating was calculated and analyzed according to Kirchhoff's law. SCTOC coating was heated to 1300 K with a high-temperature hot table, and its infrared spectrum was measured. In addition, the current–voltage (I–V) characteristic curves of the infrared spectra on a GaSb TPV cell were measured. The output power versus voltage (P–V) curves was obtained on the basis of the I–V curves and Equation (3).

$$P = V \times I \tag{3}$$

Fig. 6(a) shows the SFTOC coating infrared spectrum in the measured wavelength range of 1100–2500 nm. The spectral power density of the coating increased with wavelength. Under the same heat source temperature, the infrared spectrum intensity of SFTOC coating was nearly three times higher than that of the untreated Al_2O_3 substrate. This result indicated the excellent thermo-optical conversion characteristics of SFTOC coatings. As shown in Fig. 6

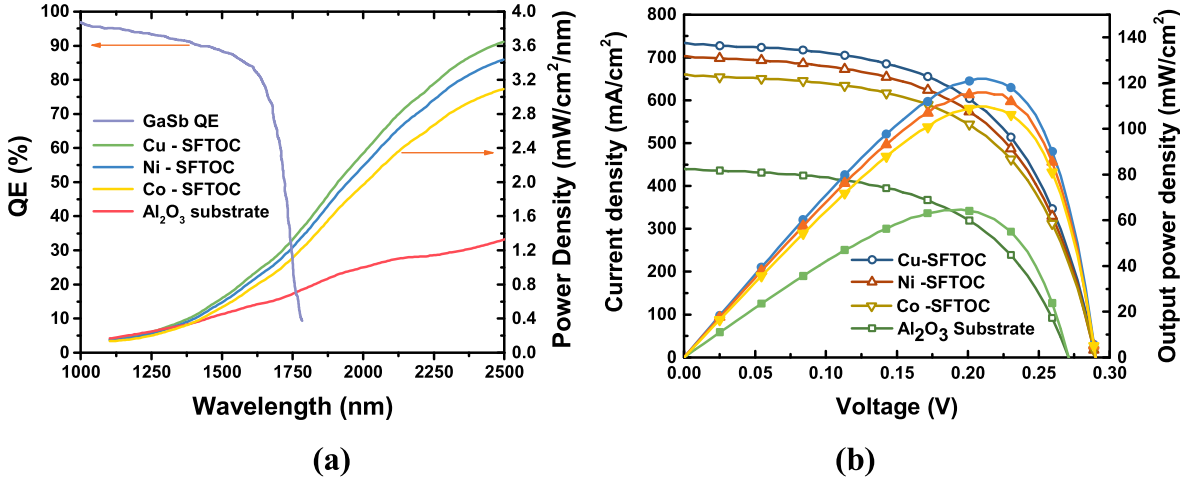

Fig. 6. (a) SFTOC coating infrared spectra and (b) I–V/P–V curves by SFTOC coating on a GaSb TPV cell at 1300 K.

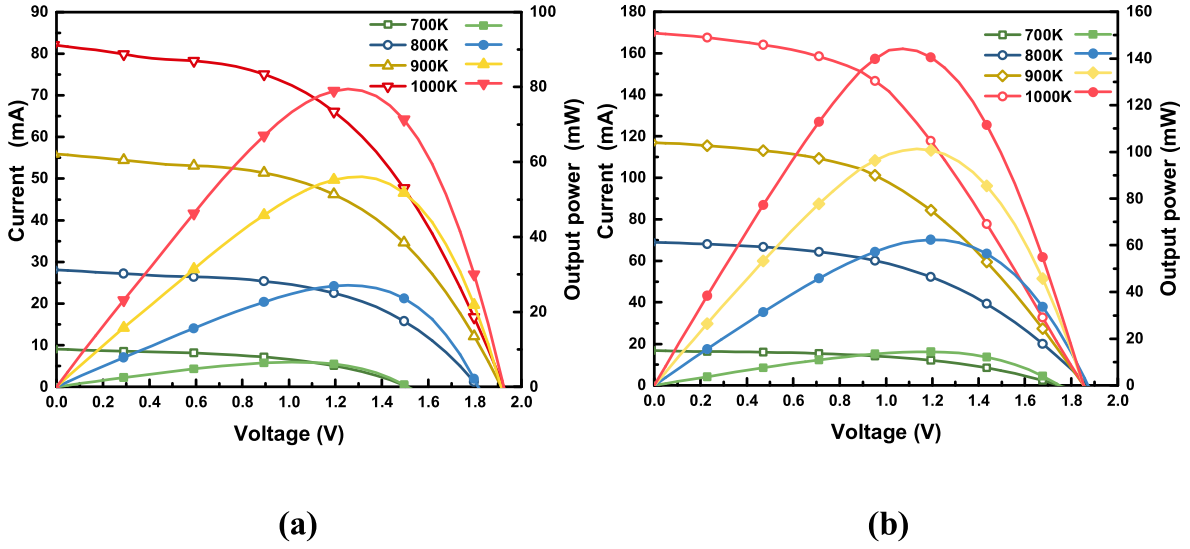

Fig. 7. *IV/PV* curve of (a) Al_2O_3 substrate and (b) Cu-SFTOC coating on a RTPV prototype.

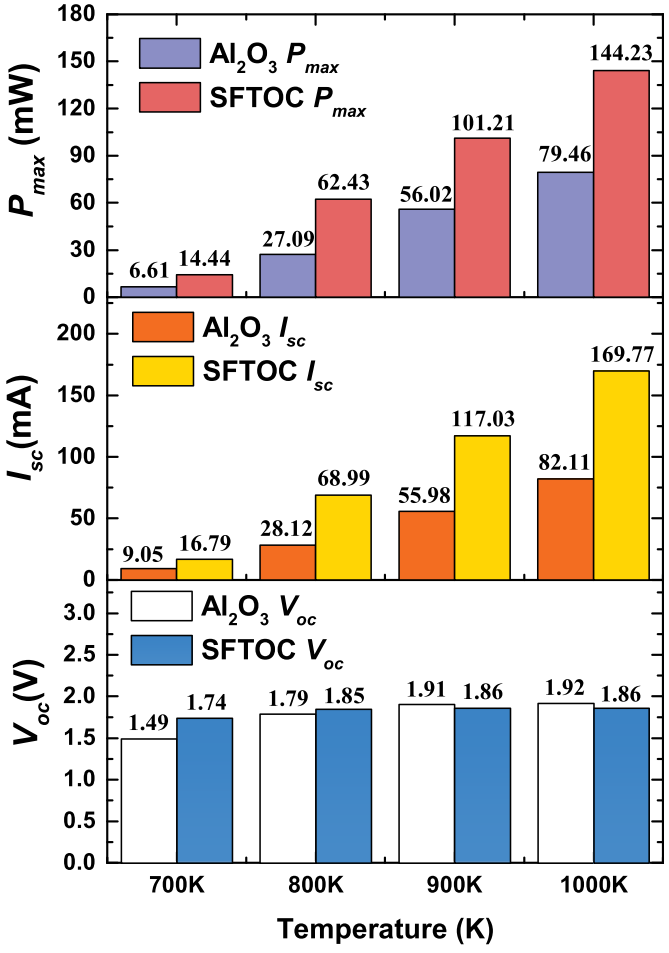

Fig. 8. Output performance comparison of the RTPV prototypes with different heat source coating.

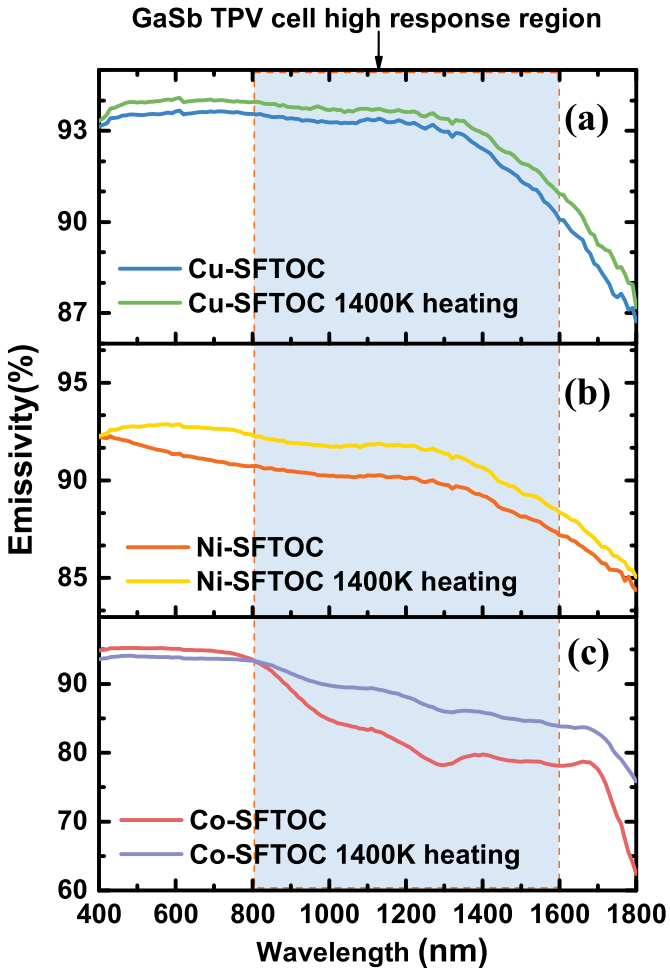

Fig. 9. (a–c) Comparison of high-temperature test of Cu/Ni/Co-SFTOC coating.

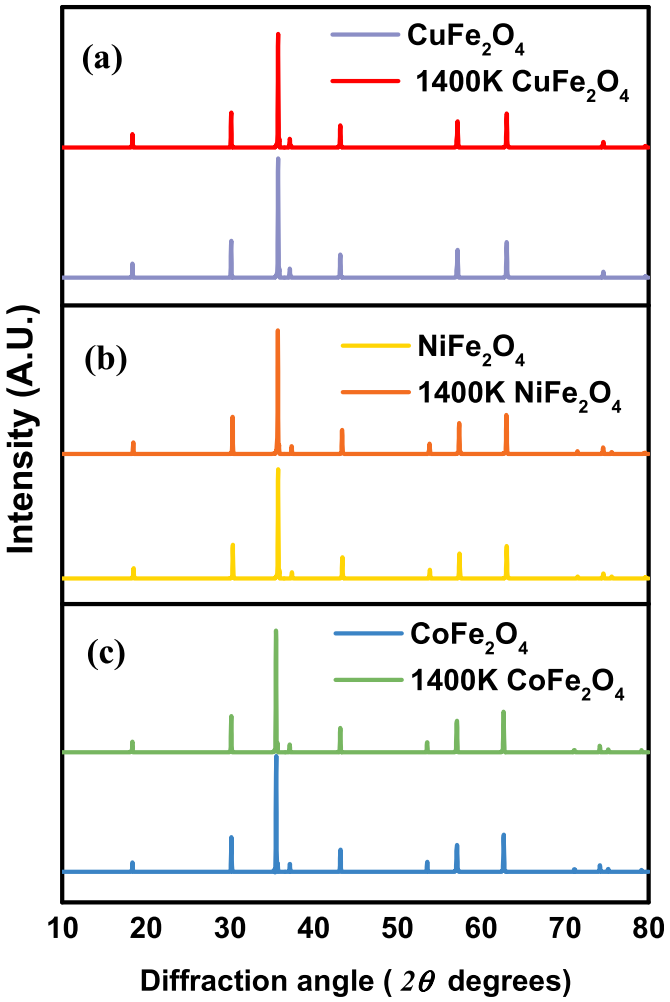

Fig. 10. (a–c) XRD of Cu/Ni/Co-SFTOC coating before and after heating.

(b), the *IV/PV* curves also show the same trend. The experimental results of the emissivity curve of the coating above can reflect that Cu-SFTOC coating achieves the highest power output. The current and output power generated by SFTOC coating in a TPV cell at 1000 K was greater than that of Al_2O_3 substrate.

The equivalent heat source coated with Cu-SFTOC was loaded into a RTPV prototype to verify the practical application advantages of SFTOC coating on RTPV. In addition, the heat source was only heated to 700 K–1000 K to ensure the temperature accuracy and repeatability of the equivalent heat source. The *IV/PV* curves of SFTOC coating at different temperatures were measured respectively. Fig. 7(a and b) show the *IV/PV* curves of Cu-SFTOC coating and Al_2O_3 substrate at different temperatures. The Cu-SFTOC coating significantly improved the infrared radiation emission efficiency of the same temperature and enabled greater current and output power. The electrical parameters, including open-circuit voltage (V_{oc}), short-circuit current (I_{sc}), and maximum output power (P_{max}), were extracted (Fig. 8). At various temperatures, I_{sc} and P_{max} of RTPV with SFTOC coating were higher than that with Al_2O_3 substrate. When the temperature of the heat source was 1000 K, Cu-SFTOC coating generated V_{oc} of 1.86 V, I_{SC} of 169.77 mA, and P_{max} of 144.23 mW. By contrast, in the Al_2O_3 substrate, I_{sc} increased to nearly 206.76%, and P_{max} increased to 181.51%. Therefore, SFTOC coating applied to RTPV can significantly improve the overall current and power output.

In addition, the V_{oc} increases slowly with the increase of heat source temperature, and the V_{oc} of SFTOC coating is even slightly lower than that of Al_2O_3 at 1000 K. On the one hand, the TPV cell has an inherent energy band gap (GaSb, $E_g = 0.72$ eV), as the radiation intensity increases, the V_{oc} tends to a saturation value. On the other hand, high temperature has certain negative effects on TPV cell. SFTOC coating has a higher emissivity, which can improve the thermal radiation intensity, accompanied by a greater amount of infrared emission, it also carries more heat deposition. As a result, the temperature of TPV cell rises, and the V_{oc} of SFTOC decreases slightly, making it slightly lower than Al_2O_3. However, the above changes of V_{oc} in this process have a weak impact on the comparison between them.

$$P_{max} = Max(V \times I) \tag{4}$$

3.3. Analysis of high-temperature tolerance of SFTOC coating

SFTOC coatings provide excellent thermo-optical emission at high temperature section (800–1300 K) and excellent electrical output for RTPV applications. Meanwhile, as an emitter, it is required to operate at high temperatures for long periods of time and to maintain a high thermo-optical emission. So the thermo-optical emission stability of SFTOC coating at high temperature must be further analyzed. After the tolerance test of SFTOC coating at 1400 K for 24 h, the emissivity of the three SFTOC coatings did not decline significantly. The overall emissivity of Ni-SFTOC coatings before and after a high-temperature test were increased by approximately 3%–4% (Fig. 9[a–c]). Based on the XRD results, the material properties of the coating did not change, and the lattice structure did not deflect (Fig. 10[a–c]).

Futhermore, the emissivity change was explored from the microscopic structure. Fig. 11(a and b) clearly shows the structural features similar to triangular dodecahedron. This structure is in accordance with the crystal configuration of spinel-type ferrite, which shows high emissivity for the SFTOC coating, thereby improving its thermo-optical conversion efficiency. By comparing the SEM images of Ni-SFTOC coating after heating, we found that the crystal shape of the surface changed into sharp tetrahedral pyramidal crystals (Fig. 11[c–d]). This phenomenon is due to the effect of high temperature, and the crystal angle on the surface of SFTOC coating becomes smaller, which is more conducive to the reflection and scattering of photons. This result improves the light-absorption and thermo-optical characteristics of the SFTOC coating. Crystal configuration increases the specific surface at the micro level, and emissivity increases at the macro level. RTPV with SFTOC

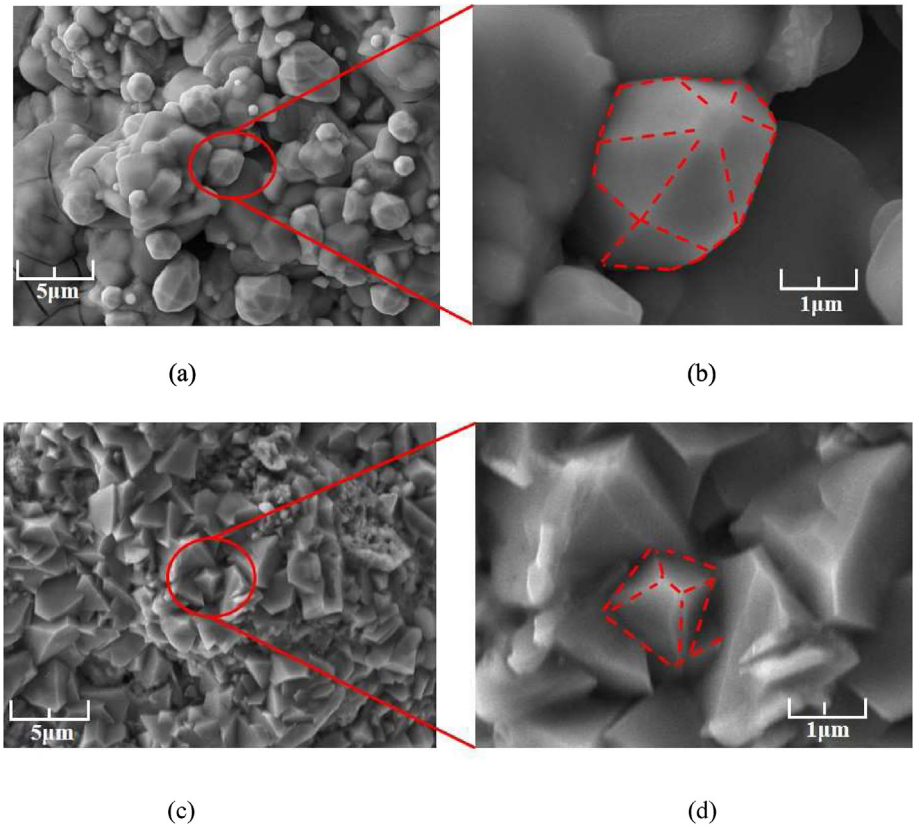

Fig. 11. SEM images of SFTOC coating before (a–b) and (c–d) after high temperaμture.

coating works in a long-term high-temperature environment of approximately 1400 K, and the thermo-optical conversion efficiency can ensure stability and evenness.

High-temperature cycle experiment was adopted to evaluate the high-temperature stability of SFTOC coating applied in RTPV. The heat source of RTPV with SFTOC coating was heated to 1000 K, and it was heated four times in a cycle within 45 min. Data was collected was conducted at 1-min intervals. The electrical parameters, including V_{oc}, P_{max}, and I_{sc} of RTPV were extracted to draw the curve of their variation trend (Fig. 12). V_{oc} and P_{max} indicate that the prepared SFTOC coating can maintain stability during the cyclic application of RTPV. This also means that SFTOC can still maintain the original output level after alternating high and low temperature working scenarios. It can be used in extreme environments such as space and polar regions.

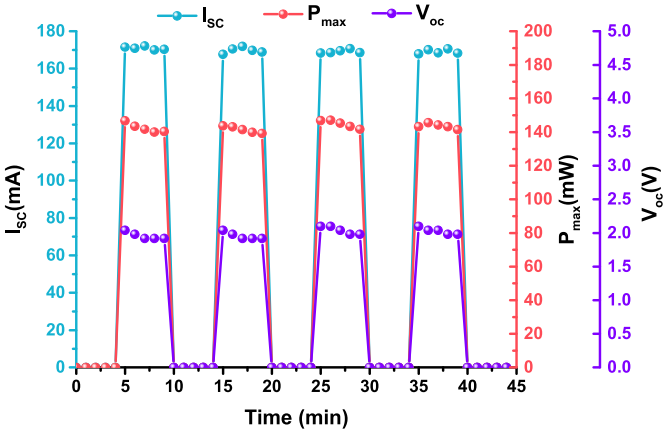

Fig. 12. The electrical parameters of V_{oc}, P_{max}, and I_{sc} changed with time curves during the cycle heating experiment.

3.4. Radiation stability analysis of SFTOC

After being irradiated at a dose rate of 0.68 kGy/h for 48 h, the surface emissivity of SFTOC coatings has not changed, and it has good tolerance to ionizing radiation (Fig. 13 [a–c]). It can be seen that the Cu/Ni-SFTOC coatings have good radiation resistance, Co-SFTOC has a 4% fluctuation range from 1200 to 1800 nm. No lattice phase transformation was observed in the XRD spectra (Fig. 14 [a–c]).The surface emissivity and thermo-optical characteristics of SFTOC coating are not changed under the action of GPHS heat source rays for 27.6 yrs. Notably, under high-temperature and strong irradiation, the adhesion characteristics of SFTOC coating are not affected. In other similar extreme circumstances, SFTOC coating

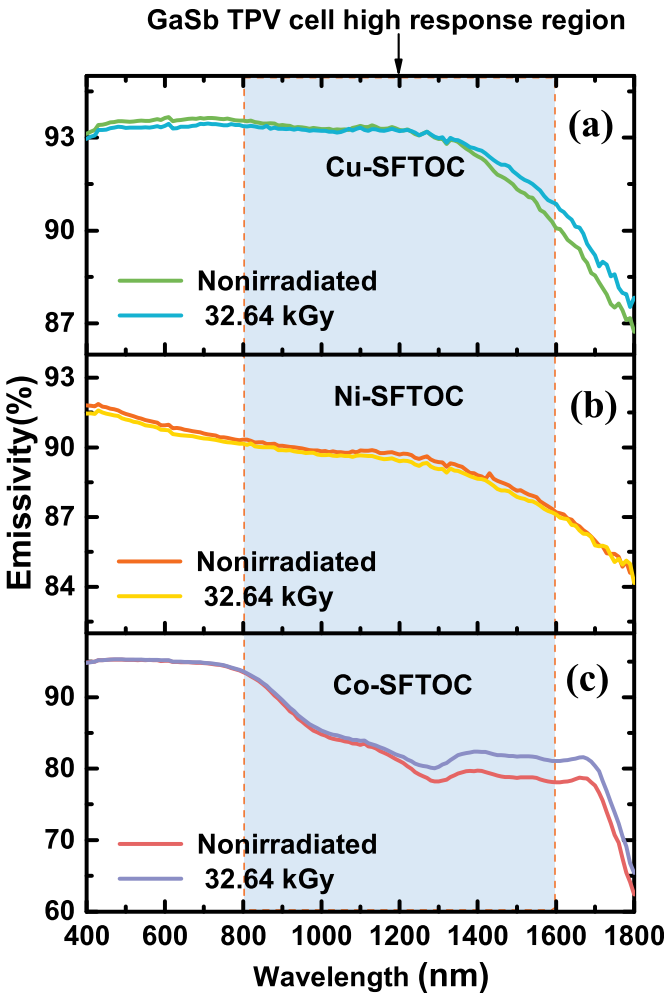

Fig. 13. (a–c) Comparison of radiation tolerance test of SFTOC coating.

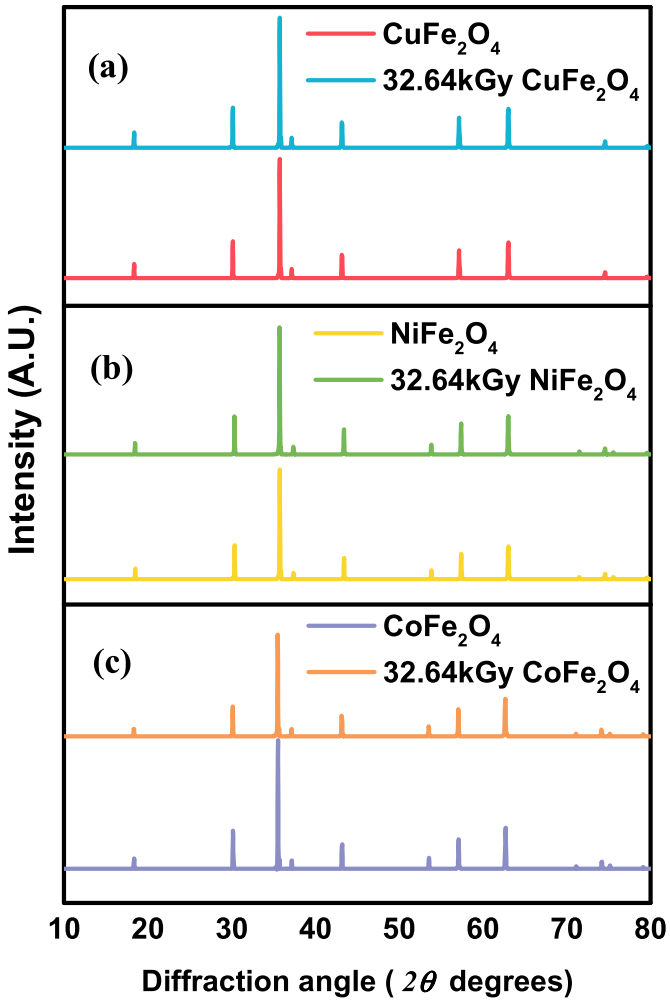

Fig. 14. (a–c) XRD of SFTOC coating before and after irradiation.

can be used as refractory protective coating.

4. Conclusions

A radioisotope heat source external SFTOC coating was developed to enhance the performance of RTPV, which possessed high-temperature (1400 K) and radiation resistance (32.64 kGy). After high-temperature heating, the crystal angle in the surface morphology of the coating was changed to form sharp crystals. Microscopically, the specific surface area of the coating was increased, and surface emissivity was increased. Under high-dose photon irradiation, emissivity had not changed. The above-mentioned experimental results showed that the prepared coating had good high-temperature and irradiation resistance. The RTPV maximum output power of SFTOC coating can reach 144.23 mW, the output performance improved 1.81 times. In the experiment of thermal shock resistance with temperature alternation, the coating can still maintain high efficiency electrical output. The SFTOC coating prepared in this study has excellent performance in improving thermo-optical conversion. It is not only suitable for the improvement of RTPV performance, but also has good application prospects in the fields of solar absorbers and refractory materials.

Credit author statement

Hongyu Wang: Methodology, Software, Formal analysis, Investigation, Resources, Writing – original draft, Visualization. **Zhiheng Xu:** Writing - Review & Editing, Funding acquisition. **Zicheng Yuan:** Methodology, Writing – review & editing. **Kai Liu:** Writing - Review & Editing. **Caifeng Meng:** Writing - Review & Editing. **Xiaobin Tang:** Writing - Review & Editing, Supervision.

Declaration of competing interest

The authors declare that they have no known competing financial interests or personal relationships that could have appeared to influence the work reported in this paper.

Acknowledgments

This work is supported by the National Natural Science Foundation of China (Grant No. 12075119), the Postgraduate Research & Practice Innovation Program of Jiangsu Province (Grant No. KYCX21_0205).

References

[1] Prelas MA, Weaver CL, Watermann ML, Lukosi ED, Schott RJ, Wisniewski DA. A review of nuclear batteries. Prog Nucl Energy 2014;75:117–48.
[2] Lange RG, Carroll WP. Review of recent advances of radioisotope power systems. Energy Convers Manag 2008;49:393–401.
[3] Yuan Z, Tang X, Xu Z, Li J, Chen W, Liu K, et al. Screen-printed radial structure micro radioisotope thermoelectric generator. Appl Energy 2018;225:746–54.
[4] Liu K, Tang X, Liu Y, Xu Z, Yuan Z, Zhang Z. Enhancing the performance of fully-scaled structure-adjustable 3D thermoelectric devices based on cold–press sintering and molding. Energy 2020;206:118096.
[5] Liu K, Tang X, Liu Y, Xu Z, Yuan Z, Ji D, et al. Experimental optimization of small–scale structure–adjustable radioisotope thermoelectric generators. Appl Energy 2020;280:115907. https://doi.org/10.1016/j.apenergy.2020.115907.
[6] Yang Z, Peng W, Liao T, Zhao Y, Lin G, Chen J. An efficient method exploiting the waste heat from a direct carbon fuel cell by means of a thermophotovoltaic cell. Energy Convers Manag 2017;149:424–31.
[7] Kim Y, Kim MJ, Kim YS, Lee H, Lee SM. Nanostructured radiation emitters: design rules for high-performance thermophotovoltaic systems. ACS Photonics; 2019.
[8] Chang CC, Kort-Kamp W, Nogan J, Luk TS, Chen HT. High-temperature refractory metasurfaces for solar thermophotovoltaic energy harvesting. Nano Lett 2018;18(12):7665–73.
[9] Lenert A, Bierman DM, Nam Y, Chan WR. Celanovi? I, Solja?I? M, et al. A nanophotonic solar thermophotovoltaic device. Nat Nanotechnol 2014;9:126.
[10] Chubb D. Fundamentals of thermophotovoltaic energy conversion (google eBook). Elsevier; 2007.
[11] Woolf DN, Kadlec EA, Bethke D, Grine AD, Hensley JM. High-efficiency thermophotovoltaic energy conversion enabled by a metamaterial selective emitter. Optica 2018;5:213.
[12] Wang X, Liang R, Fisher P, Chan W, Xu J. Radioisotope thermophotovoltaic generator design methods and performance estimates for space missions. J Propul Power 2020:1–11.
[13] Fraas L, Samaras J, Avery J, Minkin L. Antireflection coated refractory metal matched emitters for use with GaSb thermophotovoltaic generators. Conf Rec IEEE Photovolt Spec Conf 2000;2000– Janua. https://doi.org/10.1109/PVSC.2000.916059. 1020–3.
[14] Datas A, Martí A. Thermophotovoltaic energy in space applications: review and future potential. Sol Energy Mater Sol Cells 2017;161:285–96.
[15] Wang X, Liang R, Fisher P, Chan W, Xu J. Critical design features of thermal-based radioisotope generators: a review of the power solution for polar regions and space. Renew Sustain Energy Rev 2020;119:109572.
[16] Shin S, Wang Q, Luo J, Chen R. Advanced materials for high-temperature thermal transport. Adv Funct Mater 2020;30:1–23. https://doi.org/10.1002/adfm.201904815.
[17] Wang H, Tang X, Liu Y, Xu Z, Yuan Z, Liu K, et al. Thermal emission-enhanced and optically modulated radioisotope thermophotovoltaic generators. Energy Technol 2020;8. https://doi.org/10.1002/ente.201901170.
[18] Rinehart GH. Design characteristics and fabrication of radioisotope heat sources for space missions. Prog Nucl Energy 2001;39:305–19.
[19] Vining CB, Bennett GL. Power for science and exploration: upgrading the general-purpose heat source radioisotope thermoelectric generator (GPHS-RTG). 8th Annu Int Energy Convers Eng Conf 2010. https://doi.org/10.2514/6.2010-6598.
[20] Lee J, Cheon S, Hong S, Nam Y. A radioisotope thermophotovoltaic converter with nanophotonic emitters and filters. Int J Heat Mass Tran 2017;108:1115–25. https://doi.org/10.1016/j.ijheatmasstransfer.2016.12.049.
[21] Cheon SJ, Hong SG, Lee JH, Nam YS. Design and performance analysis of a 500-W heat source for radioisotope thermophotovoltaic converters. Int J Energy Res 2018;42:817–29. https://doi.org/10.1002/er.3889.
[22] Brown EJ, Baldasaro PF, Burger SR, Danielson LR, Depoy DM, Dolatowski JM, et al. Status of thermophotovoltaic energy conversion technology at lockheed martin corp. Off Sci Tech Inf Tech Rep 2004:5676.
[23] Sakakibara R, Stelmakh V, Chan WR, Ghebrebrhan M, Joannopoulos JD, Soljačić M, et al. Practical emitters for thermophotovoltaics: a review. J Photon Energy 2019;9:1. https://doi.org/10.1117/1.jpe.9.032713.
[24] Celanovic I, O'Sullivan FM, Ilak M, Kassakian JG, Perreault DJ. Design and optimization of one-dimensional photonic crystals for thermophotovoltaic applications. Opt Lett 2004;29:863–5.
[25] Molesky S, Dewalt CJ, Jacob Z. High temperature epsilon-near-zero and epsilon-near-pole metamaterial emitters for thermophotovoltaics. Opt Express 2012;21.
[26] Lin SY, Moreno J, Fleming JG. Three-dimensional photonic-crystal emitter for thermal photovoltaic power generation. Appl Phys Lett 2003;83:380–2.
[27] Zhang J, Bai H, Wei W, Ding Y, Zhang X, Yuan H, et al. The effect of microstructure on the middle and short waveband emissivity of CuO-doped $Cu_xCo_{1-x}Fe_2O_4$ spinel. J Alloys Compd 2019;787:638–48.
[28] Zhang J, Bai H, Han Y, Wang F, Zhang Z. The effect of $CuFe_2O_4$ ferrite phase evolution on 3–5 μm waveband emissivity. Ceram Int 2019;46.
[29] Fowles Grant R. Introduction to modern optics. Am J Phys 1975;36:770.
[30] Maccione L. Radiative processes in astrophysics. 2009.